Supplemental Information

# A Noelin-organized extracellular network of proteins required for constitutive and context-dependent anchoring of AMPA-receptors

Sami Boudkkazi, Jochen Schwenk, Naoki Nakaya, Aline Brechet, Astrid Kollewe, Harumi Harada, Wolfgang Bildl, Akos Kulik, Lijin Dong,Afia Sultana, Gerd Zolles, Uwe Schulte, Stanislav Tomarev and Bernd Fakler

Inventory


- Figure S1 (related to Figure 1)
- Figure S2 (related to Figures 1-5)
- Figure S3 (related to Figure 1)
- Figure S4 (related to Figure 2)
- Figure S5 (related to Figure 2)
- Figure S6 (related to Figure 2)
- Figure S7 (related to Figure 2)
- Figure S8 (related to Figure 3)
- Figure S9 (related to Figure 4)
- Figure S10 (related to Figure 4, Discussion)
- Figure S11 (related to Figure 5)
- Figure S12 (related to Figure 6, Discussion)
- Figure S13 (related to Figure 6, Discussion)
- Figure S14 (related to STAR Methods, Discussion)

**Figure S1**

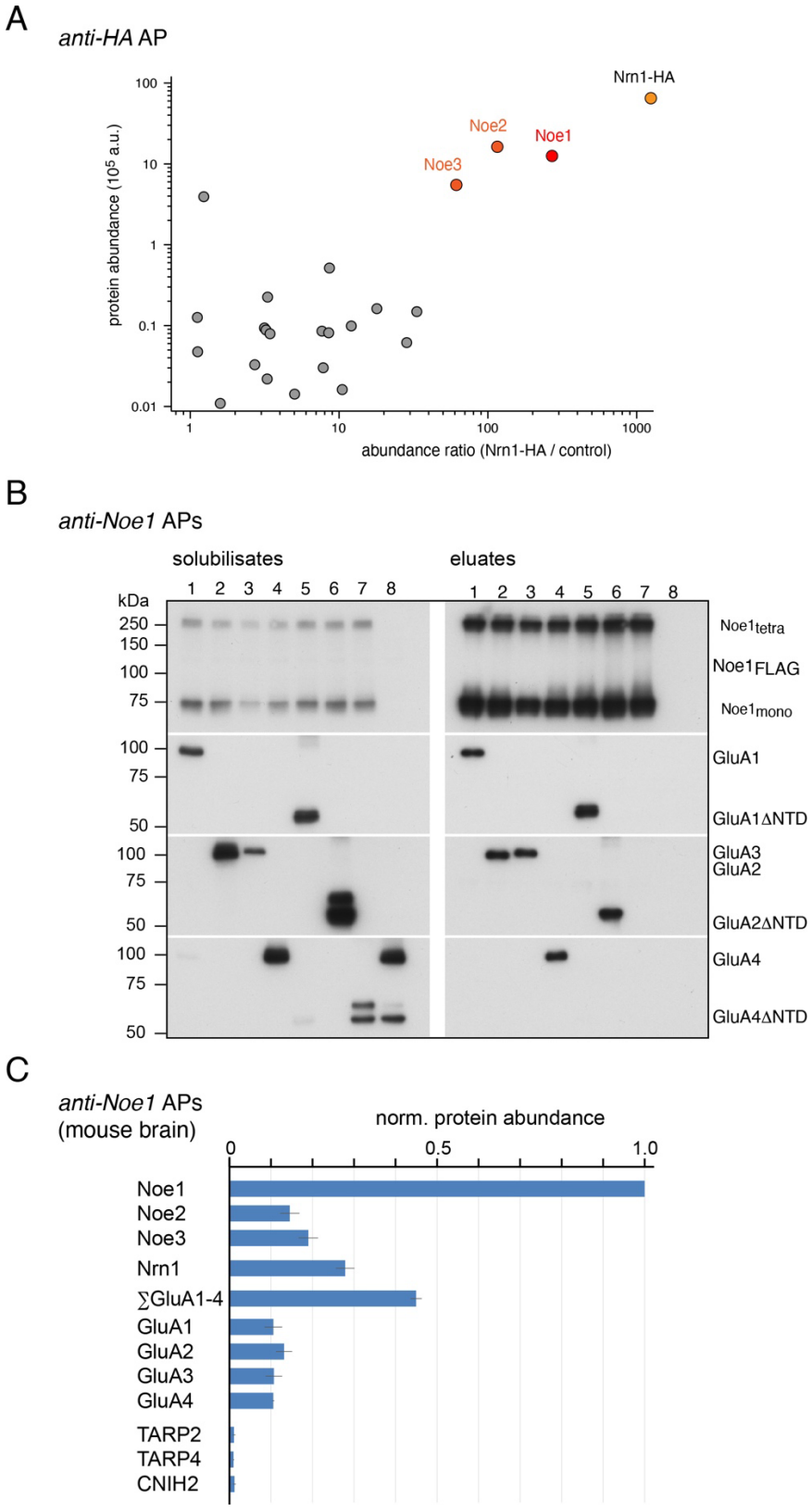


**Figure S1**

**Binding of Noelins1-3 to Neuritin and AMPARs**. (related to Figure 1)

(**A**) Cultured cortical neurons were transduced with AAV-virus driving expression of HA-tagged Neuritin or GFP (used as a control). CL-47 solubilized protein complexes

were isolated at DIV21 with anti-HA antibodies and eluates analyzed by mass spectrometry. Note that HA-tagged Neuritin and Noe1, 2 and 3 were specifically (co)-purified (abundance ratio) and by far the most abundant proteins detected in the eluate (protein abundance). (**B**) Noe1-binding to all GluA subunits: Noe1 was transiently co-expressed in tsA201 cells with GluA1, A2, A3, A4 (Lanes 1-4), GluA1-, A2-, A4ΔNTD (Lanes 5-7); sole expression of GluA4 and GluA4ΔNTD was used as specificity control (Lane 8). Protein complexes were isolated with *anti-Noe1* ABs. Input of CL-91 solubilisates and AP-eluates were separated by SDS-PAGE and Western-probed for the indicated proteins. ΔNTD refers to deletion of the N-terminal domain of GluAs 1, 2 and 4 (Watson et al., 2017). Note that all GluA proteins were robustly co-purified with FLAG-tagged Noe1, except for GluA4ΔNTD.
(**C**) Effective co-purification of AMPARs in *anti-Noe1* APs from CL-91 solubilized membrane fractions from the entire adult mouse brain. MS-determined abundance values for the indicated proteins were normalized to the amount of Noe1.

**Figure S2**

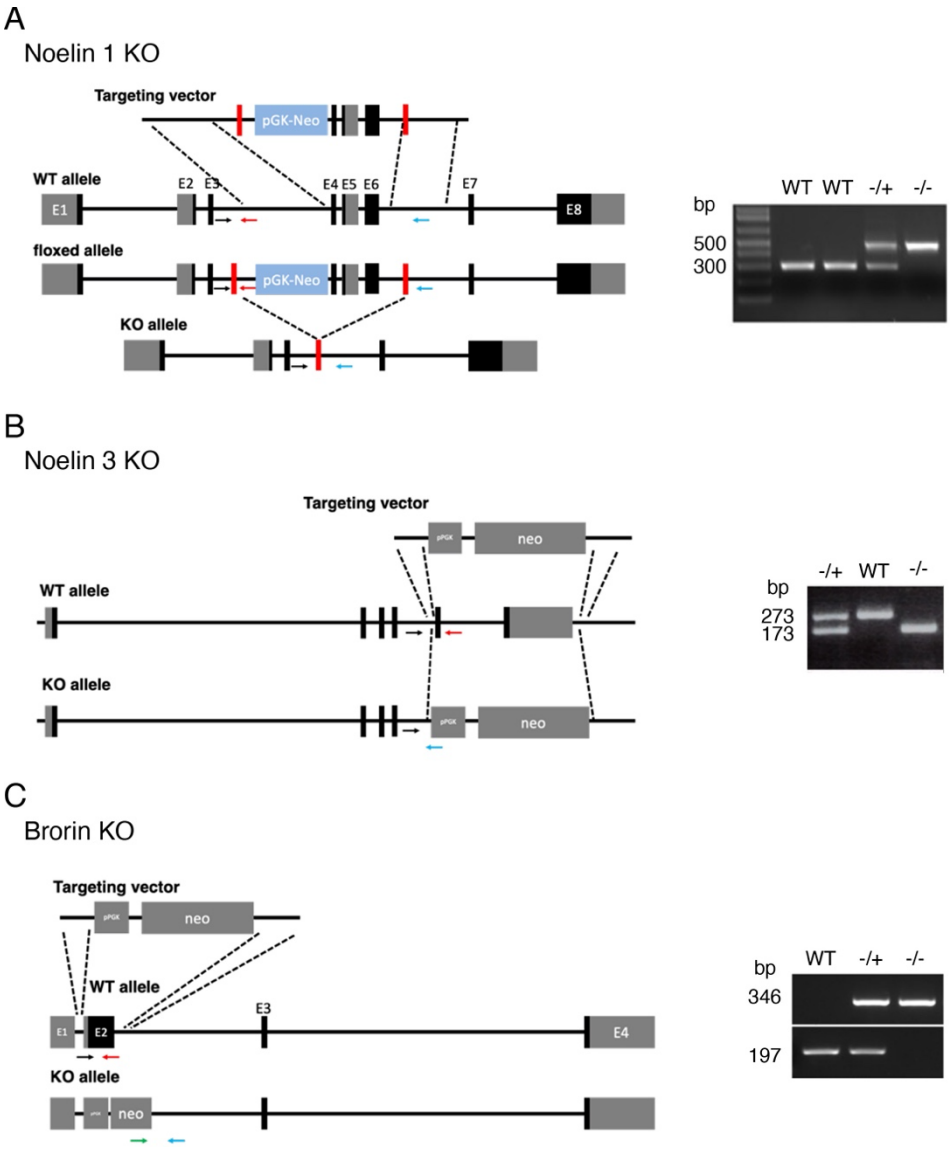

**Figure S2**

**Diagrams illustrating production of Noe1, Noe 3, and Brorin KO mice**.

(related to Figures 1-5)

(**A**) Design of the targeting vector and resulting structure of the modified *Olfm1* gene after two recombination events (left); PCR genotyping results of *Olfm1* WT (308 bp) and KO (469 bp) alleles (right). Red bars represent loxP sites. (**B**) Design of the targeting vector and resulting structure of the modified Olfm3 gene after a recombination event (left); PCR genotyping results of *Olfm3* WT (273 bp) and KO (173 bp) alleles (right). (**C**) Brorin KO mouse (MMRRC-UC-Davis). The first coding exon (exon2) was eliminated using a targeting vector (left); PCR genotyping results of Brorin WT and KO alleles (right). Black, red and blue arrows represent common forward, wildtype reverse and knockout reverse primers for PCR genotyping, respectively.

**Figure S3**

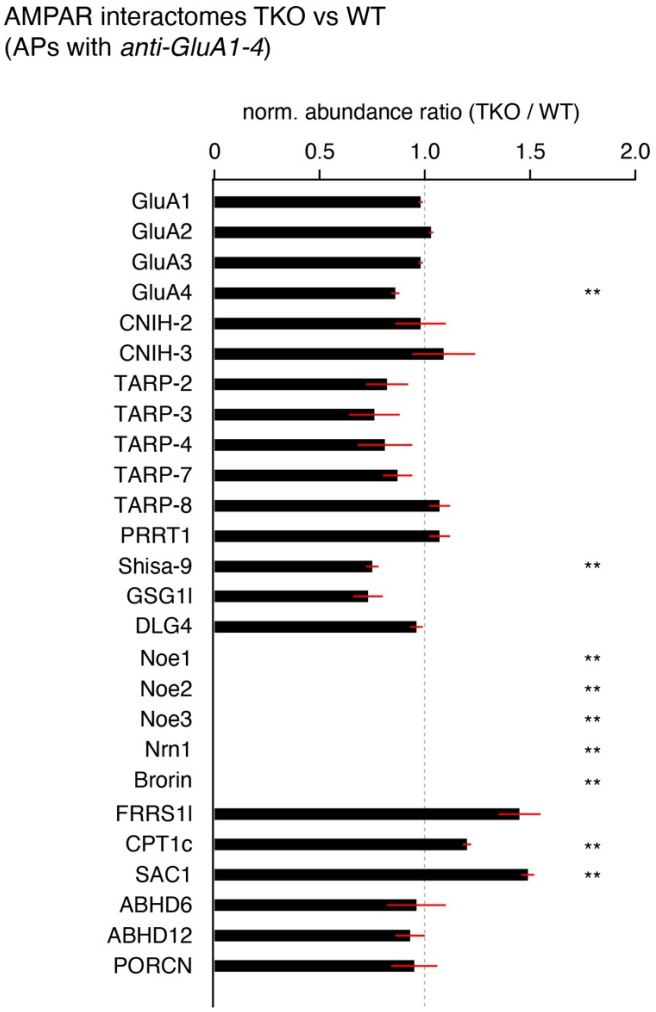


**Figure S3**

**Comparative AMPAR interactomes determined from WT and Noe1-3 TKO mice**.

(related to Figure 1)

AMPAR complexes were affinity-purified with anti-GluA1-4 antibodies from CL-47 solubilized membrane fractions prepared from TKO and WT brains (Fig. 1D).

Differences in the degree of association of interactome constituents were visualized by plotting abundance ratios between TKO and WT, calculated with abundance values normalized to the sum of GluA1-4 proteins in each AP. Note, that all extracellular and secreted proteins were lost in AMPARs from TKO brains. In addition, co-assembly of the biogenesis-factors (FRRS1l, CPT1c and Sac1) appeared increased, in TKO animals. Data are mean ± SEM of three experiments (**, p-values <0.01 for two-sided Student's T-test).

**Figure S4**

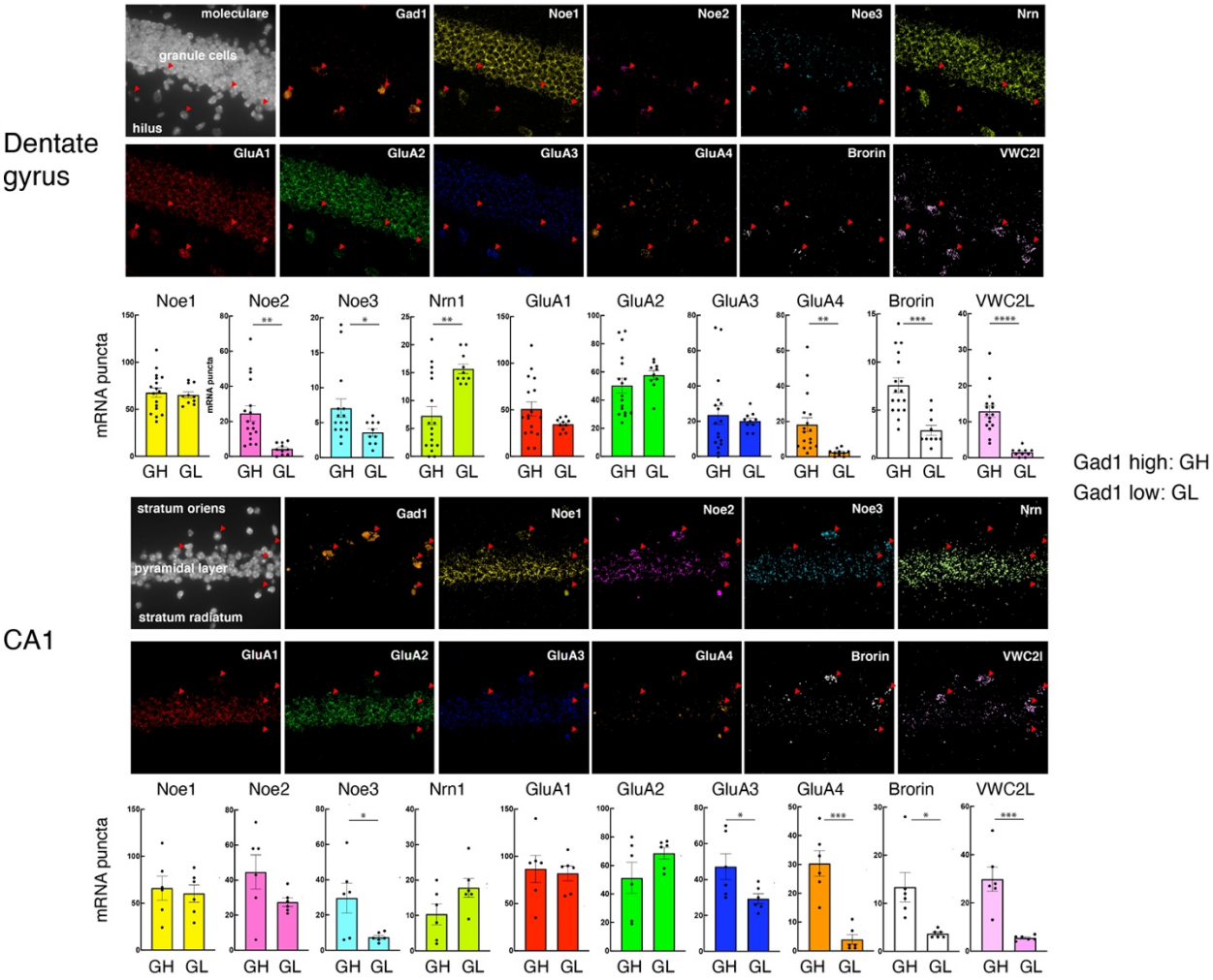


**Figure 4**

**RNAScope *in situ* hybridization with probes specific for the indicated constituents of the AMPAR interactome**. (related to Figure 2)

Representative images illustrating gene expressions in the dentate gyrus (upper panel) and CA1 region (lower panel). The number of mRNA puncta for each gene in 17 GAD1-positive (GH, more than 10 GAD1 mRNA puncta) and 10 randomly selected GAD1-non-positive (GL) cells. Arrowheads represent locations of GAD1-positive cells. Data are mean ± SEM. **** p<0.0001, ***<0.001, **<0.01 and *<0.05, respectively. Statistical analysis was performed by Student's t-test for each probe.

**Figure S5**

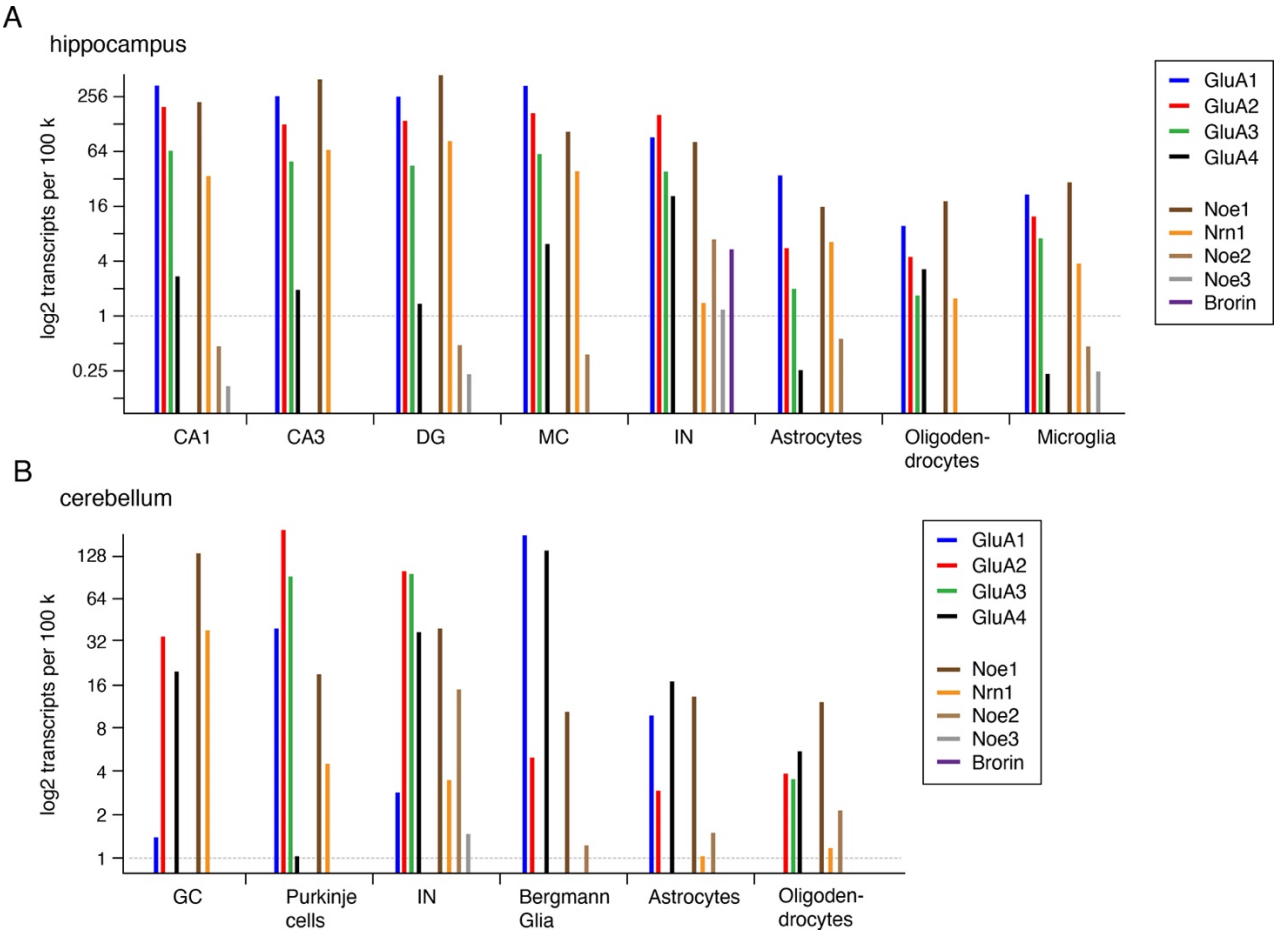


**Figure S5**

**Expression pattern of GluAs and extracellular interactors** (related to Figure 2)
Number of RNA transcripts per 100000 unique molecular identifiers in the indicated hippocampal (**A**) or cerebellar (**B**) meta-groups according to DropViz single-cell transcriptomics data [37]. CA1: CA1 pyramidal cells, CA3: CA3 pyramidal cells, DG: dentate gyrus, MC: mossy cells, IN: interneurons, GC: granule cells.

**Figure S6**

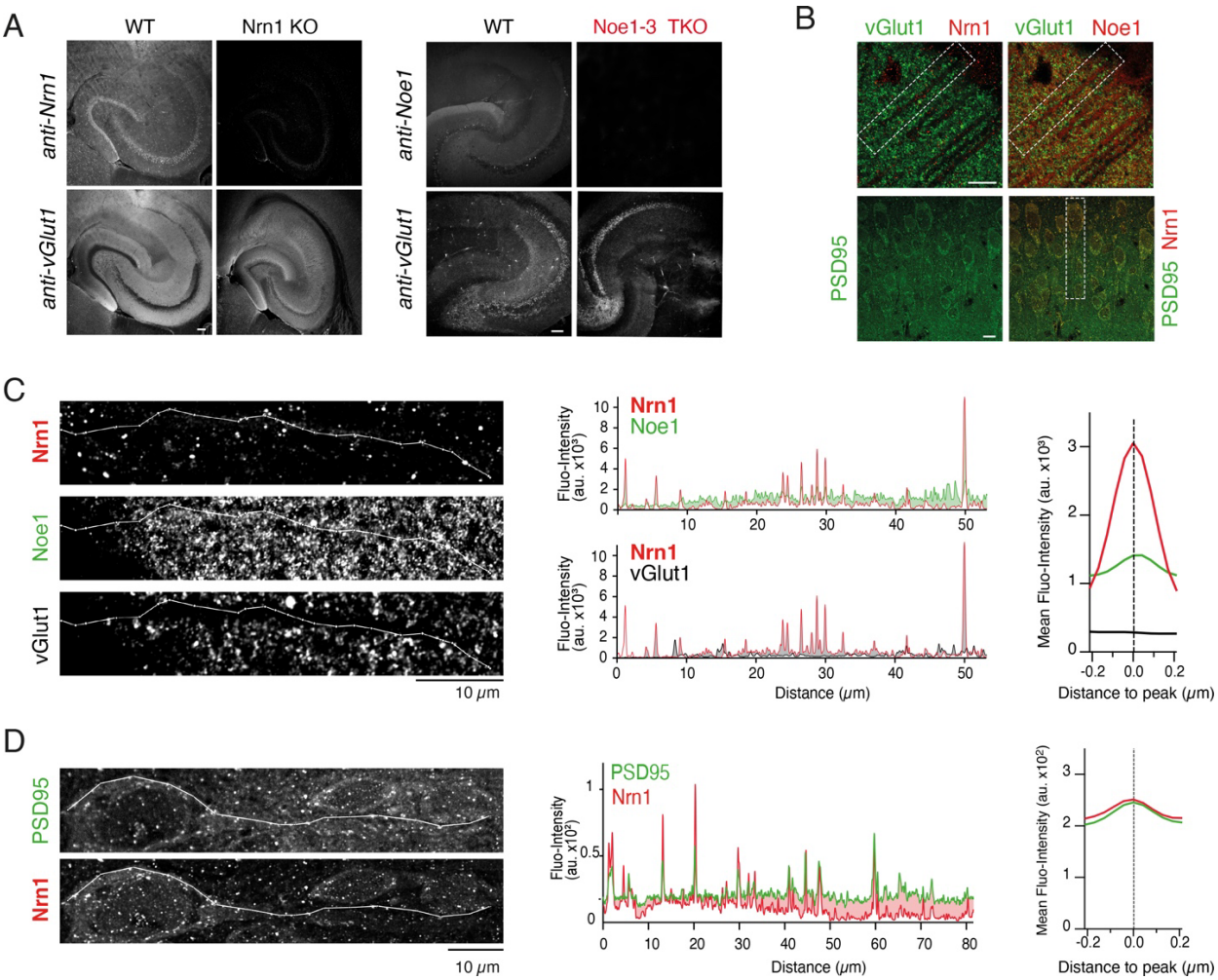


**Figure S6**

**Subcellular localization of Neuritin and Noelin1 in hippocampal CA1 pyramidal cells**. (related to Figure 2)

(**A**) Representative confocal fluorescence images of the hippocampal region in WT, Nrn1 KO and Noe1-3 TKO mice stained with ABs targeting Nrn1, Noe1 and the pre-synaptic protein vGlut1. Note the specificity of the *anti-Nrn* and *anti-Noe1* ABs for their target. Scale bars are 100 µm. (**B**) Representative confocal fluorescence images acquired with the Airyscan technique of super-resolution microscopy of somata and principal dendrites of CA1 PCs co-stained with *anti-vGlut1* (green) and either *anti-Nrn1* (red) or *anti-Noe1* (red) in the upper panel, or with *anti-PSD95* (green) and *anti-Nrn1* (red) in the lower panel. Scale bars are 10 µm. (**C**) Left panel, framed sections from the upper panel in (B) at extended scale. A reference line was drawn through the fluorescence peak signals of Nrn1 in close proximity to a putative principal dendrite, and transferred to the images obtained with *anti-Noe1* and *anti-vGlut* stainings. Middle panel, overlay of fluorescence intensity signals determined along the reference lines. Right panel, mean fluorescence intensities obtained at/around the reference peaks (± 172 nm). (**D**) Images (left), intensity signals (middle) and mean fluorescence around the peaks as in (C) but for the PSD95 (reference) and Nrn1 stainings in the lower panel

of (B). Note the tight overlap of Nrn1 with PSD95, and the partial overlap between Nrn1 and Noe1.

**Figure S7**

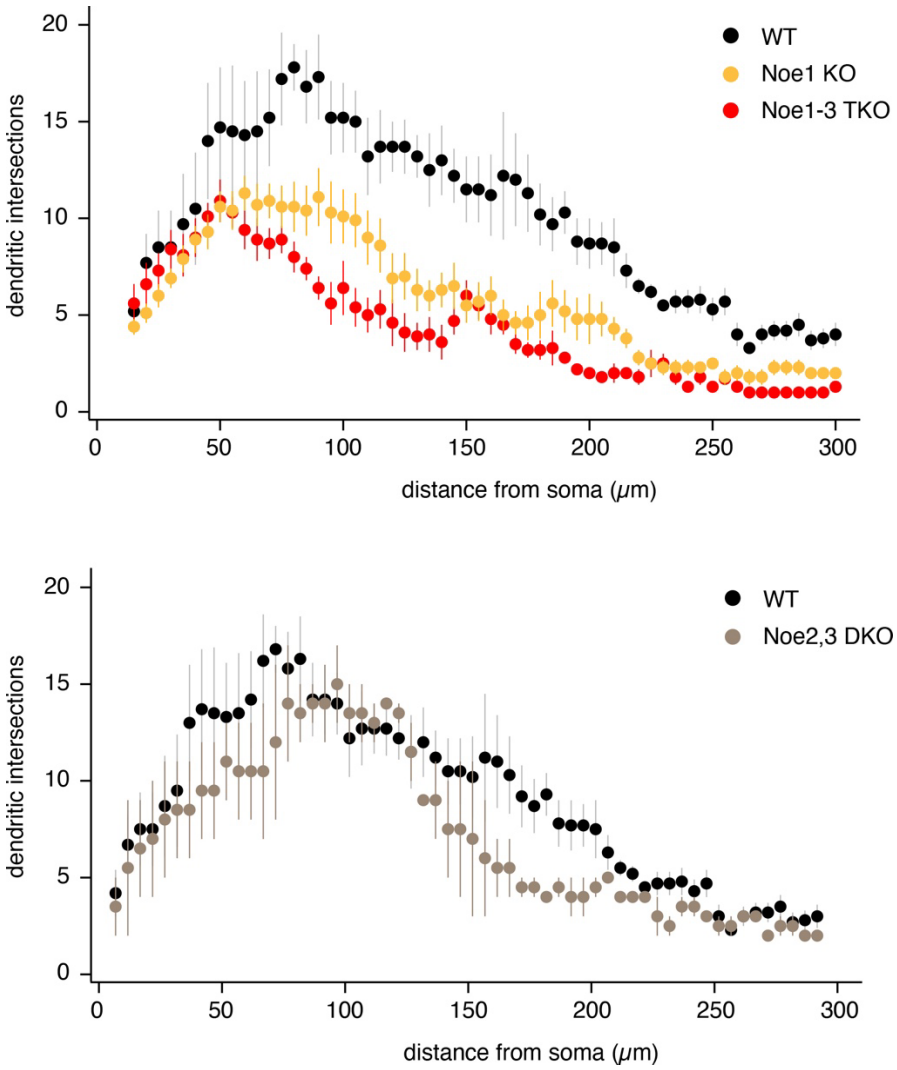


**Figure S7**

**Sholl-analysis of dendritic complexity in the principal dendrite of CA1 pyramidal cells**. (related to Figure 2)

Dendritic intersections determined as a function of the distance from soma in reconstructed CA1 PCs (as in Fig. 2B) from WT (black), Noe1 KO (yellow), Noe1-3 TKO (red) and Noe2,3 DKO (brown) mice. Data are mean ± SEM 12, 7, 7, 4 cells for WT, TKO, Noe1 KO and Noe2,3 DKO, respectively. Note the specific decrease in dendritic complexity observed in TKO and Noe1 KO neurons.

**Figure S8**

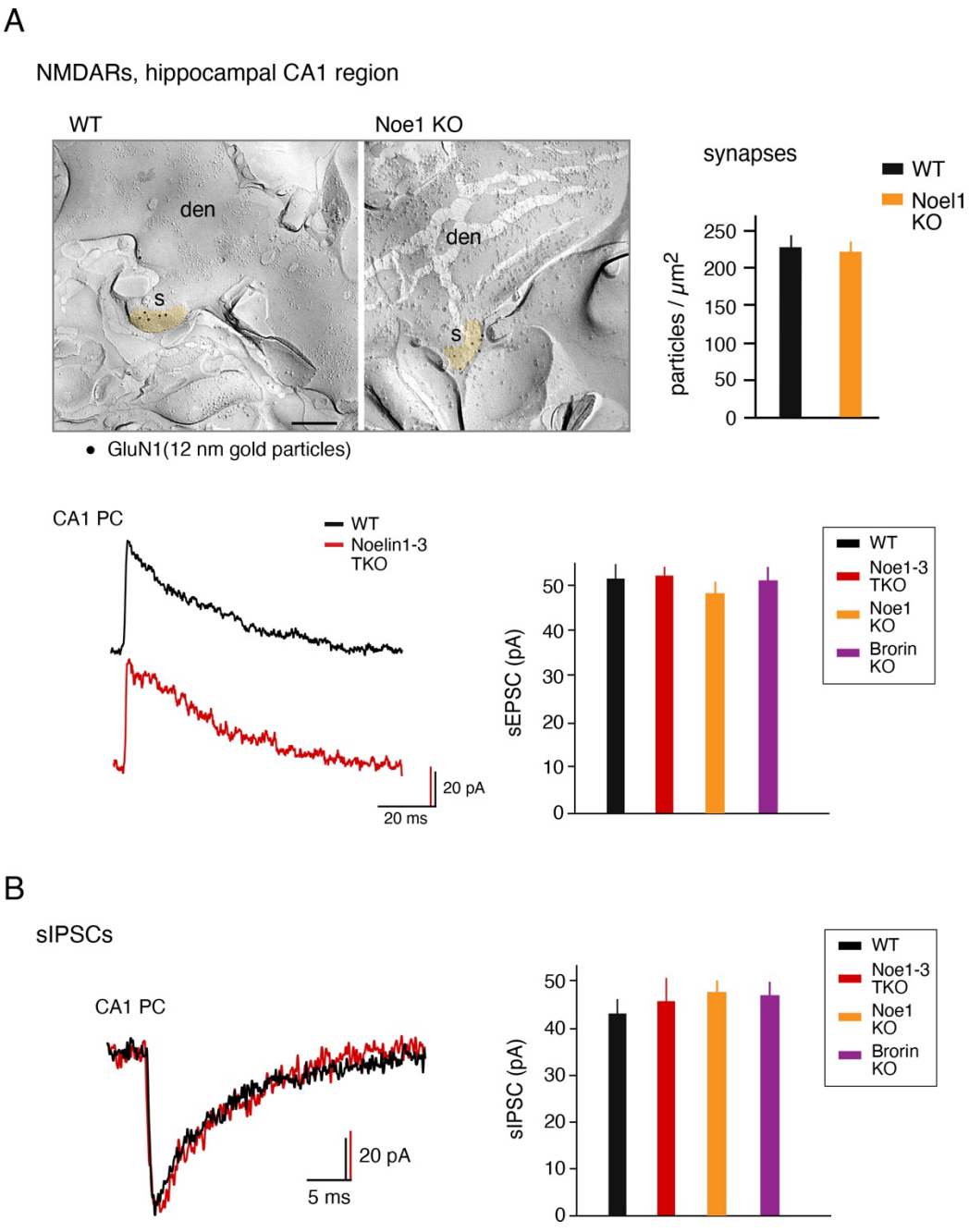


**Figure S8**

**Distribution and spontaneous EPSCs through NMDA receptors and IPSCs in hippocampal CA1 PCs.** (related to Figure 3)

(**A**) Upper left panel, electron micrographs as in Figures 2, 5 illustrating distribution of immuno-particles for the NMDA-receptor subunit GluN1 (NMDAR1, 12 nm) on the plasma membrane of spines (s) of CA1 PCs in hippocampi of WT and Noe1 KO mice. Scale bars are 200 nm. Upper right panel, bar graph summarizing surface densities of GluN1 in synapses (mean ± SD of 45 and 74 synapses (WT, Noe1 KO). Lower panel, representative NMDAR-mediated sEPSCs recorded at 40 mV in CA1 PCs of WT and TKO animals (left) and bars illustrating the sEPSC amplitudes (mean ± SEM of 10

neurons) determined in WT and the indicated KO animals. (**B**) Results as in (A), lower panel but for spontaneous IPSCs recorded at -70 mV in CA1 PCs. Data are mean ± SEM of 10 (WT), 11 (TKO), 12 (Noe1 KO) and 10 (Brorin KO) neurons.
Note the lack of effect of the Noelin KOs on both sEPSCs through NMDARs and sIPSCs through $GABA_A$ receptors.

**Figure S9**

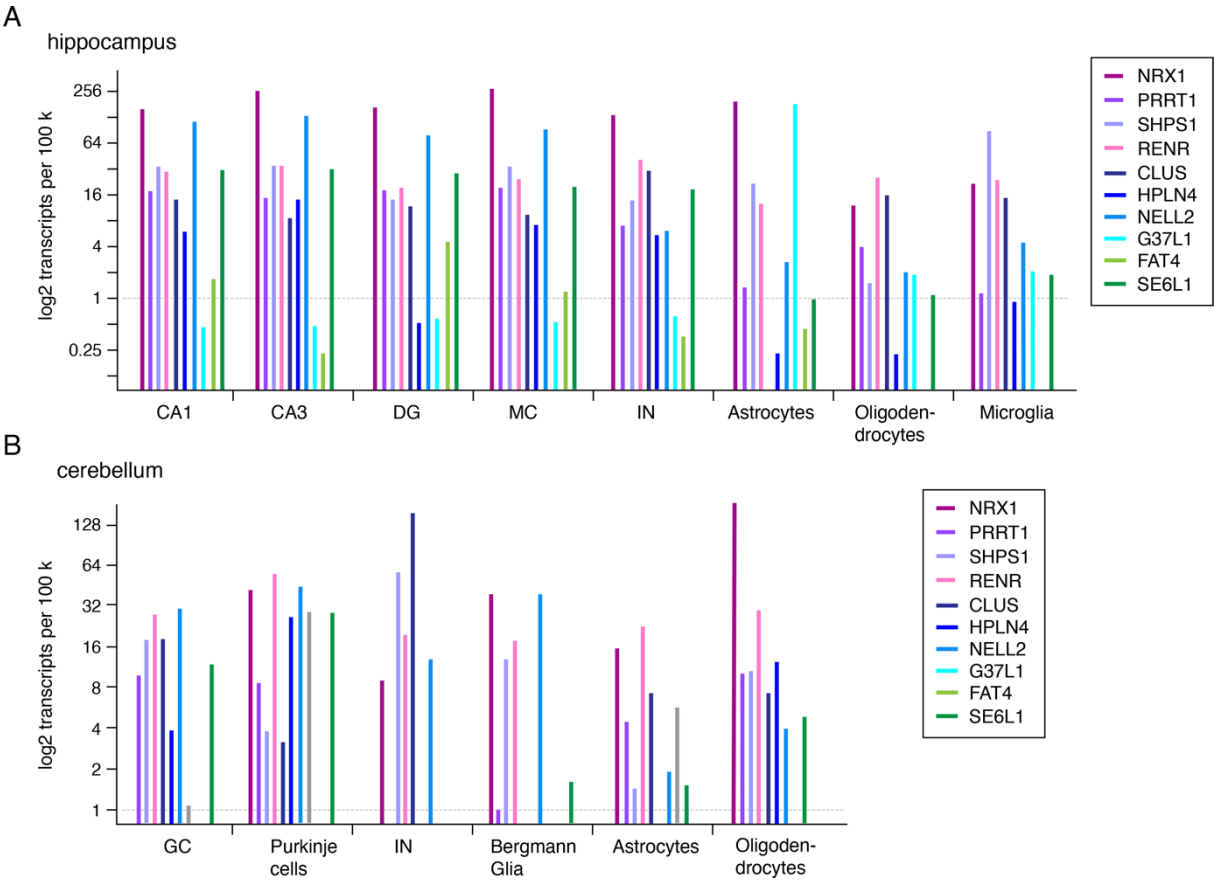


**Figure S9**
**Expression pattern of identified network constituents** (related to Figure 4)
Number of RNA transcripts per 100000 unique molecular identifiers in the indicated hippocampal (**A**) or cerebellar (**B**) meta-groups according to DropViz single-cell transcriptomics data (as in fig. S6). CA1: CA1 pyramidal cells, CA3: CA3 pyramidal cells, DG: dentate gyrus, MC: mossy cells, IN: interneurons, GC: granule cells.

**Figure S10**

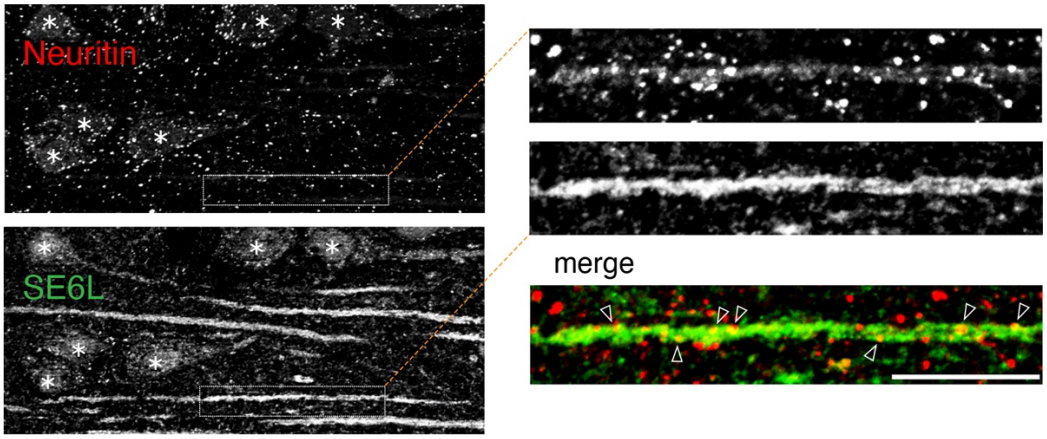


**Figure S10**

**Subcellular localization of SE6L1 in hippocampal CA1 pyramidal cells**.

(related to Figure 4, Discussion)

Confocal fluorescence images as in Figure S6 of the pyramidal cell layer in the hippocampal CA1 region stained for Nrn1 (*anti-Nrn1* AB, red) and SE6L1 (*anti-SE6L* AB, green). Left panel, overview, right panel, extension of the frames on the left. Note partial co-localization of SE6L1 (homogenously distributed along the dendrite) with the mostly spine-restricted Nrn1. Scale bar is 50 µm.

**Figure S11**

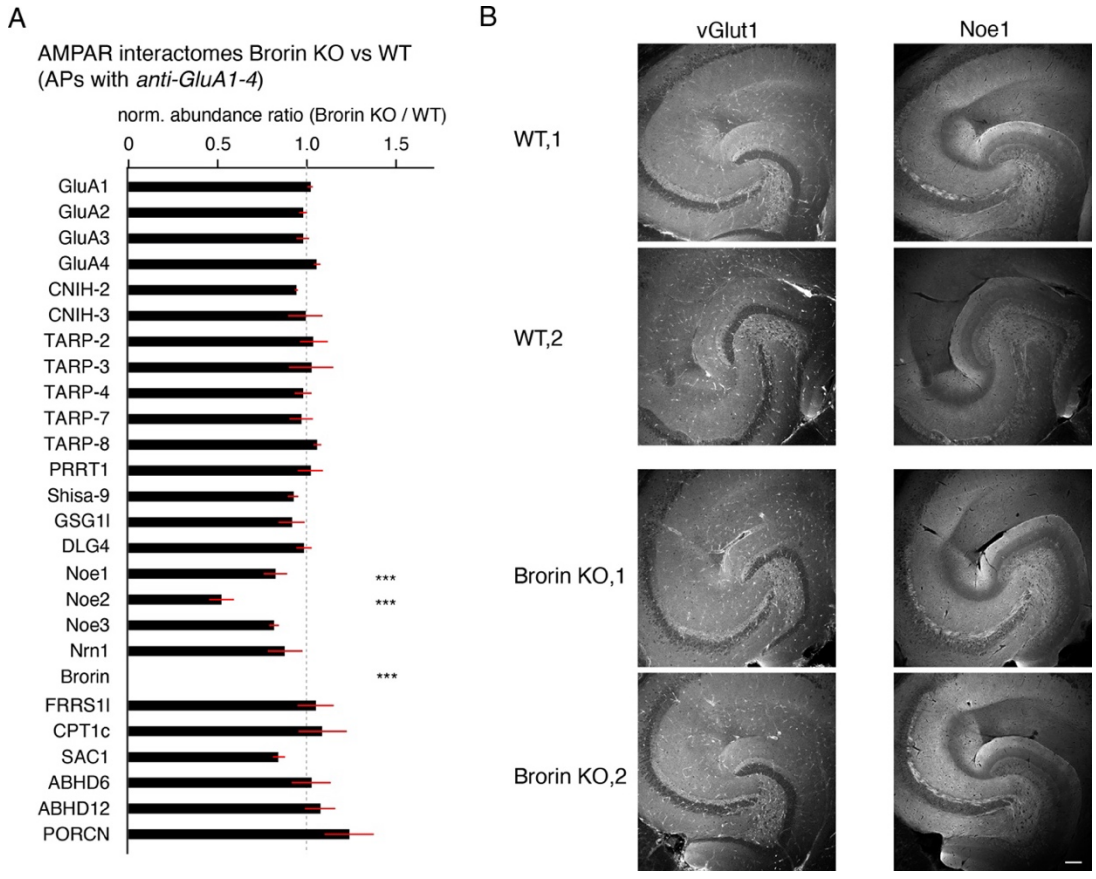

**Figure S11**

**Interactome and distribution of Noe1 in Brorin KO mice**. (related to Figure 5)
(**A**) Comparative AMPAR interactomes determined from WT and Brorin KO mice as in Figure S4. AMPAR complexes were affinity-purified with anti-GluA1-4 antibodies from CL-91 solubilized membrane fractions prepared from Brorin KO and WT brains. Differences in the degree of association of interactome constituents were visualized by plotting abundance ratios between Brorin KO and WT, calculated with abundance values normalized to the sum of GluA1-4 proteins in each AP. Note, that Noelins appeared distinctly decreased in Brorin KO animals. Data are mean ± SEM of three experiments (**, p-values <0.01 for two-sided Student's T-test). (**B**) Representative confocal images of hippocampal sections from two WT mice (1 and 2) and two Brorin KO mice (1 and 2) stained with the presynaptic marker vGlut1 (as a control, left panel) and Noe1 (right panel). Scale bar (lower left image) is 100 µm.

**Figure S12**

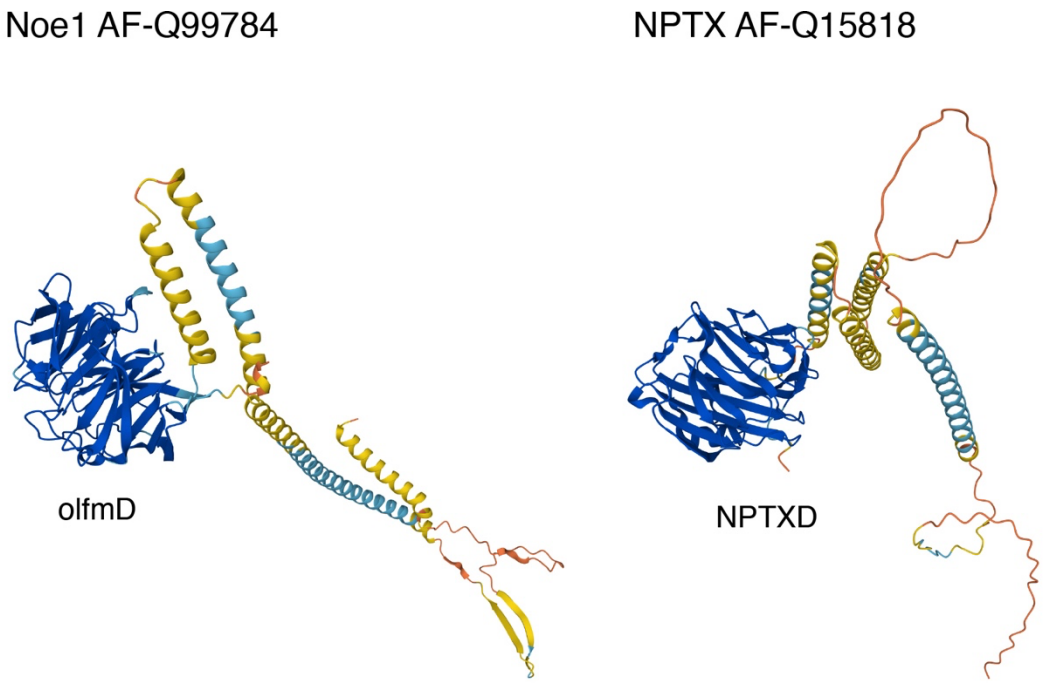


**Figure S12**

**Structural similarities between Noe1 and NPTX**. (related to Figure 6, Discussion)
Three-dimensional structures of Noe1 (left) and neuronal pentraxin 1 (right) as predicted by AlphaFold; olfmD and NPTXD are olfactomedin and pentraxin domains, respectively. Note the similarity of both structures in the aforementioned domains, as well as in the overall arrangement and folding.

**Figure S13**

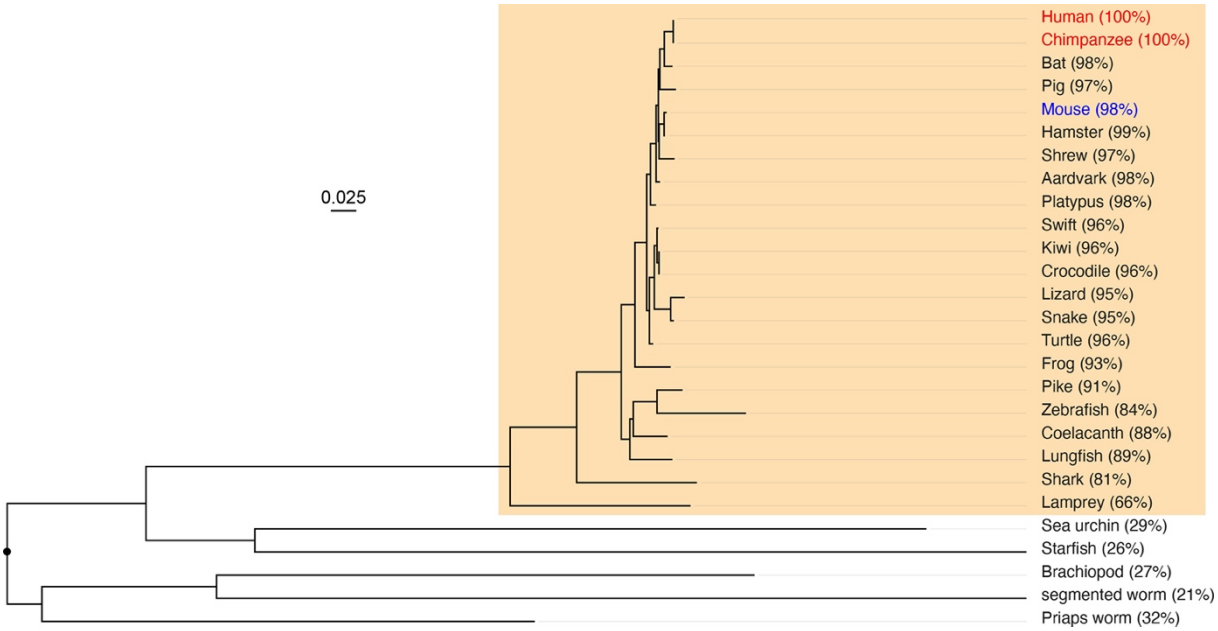


**Figure S13**
**Phylogenetic tree of noelin-1 homologs.** (related to Figure 6, Discussion)
Phylogram of proteins from various vertebrate and non-vertebrate organisms with homology to both, the Noelin-1 domain (aa 55-152) and the olfm domain (aa 226-478) of human Noe1. Amino acid sequence identity with human Noe1 is given in parentheses, scale bar indicates the average number of amino acid exchanges per site/position over the length of the branch line. Important note: Non-vertebrate Noe1 homologs with sequence identities higher than presented in the phylogram could not be identified in the BLASTP searches. Accession numbers of the identified proteins are as follows human: Q99784, chimpanzee: XP016817534, bat: XP_019612326, pig: XP_020927321, mouse: O88998, hamster: XP_005085465, shrew: XP_006165326, aardvark: XP_007952481, platypus: XP_028919103, swift: XP_009997152, kiwi: XP_013811392, crocodile: XP_019396459, snake: XP_015676630, lizard: XP_044309124, turtle: XP_006120815, frog: XP_018084524, pike: XP_039618555, zebrafish: NP_001314808, coelacanth: XP_005987466, lungfish: XP_043914239, shark: XP_041048845, lamprey: XP_032814626, starfish: XP_033645577, sea urchin: NP_999798, brachiopod: XP_013409749, segmented worm: CAH1801862, priaps worm: XP_014671171.

**Figure S14**

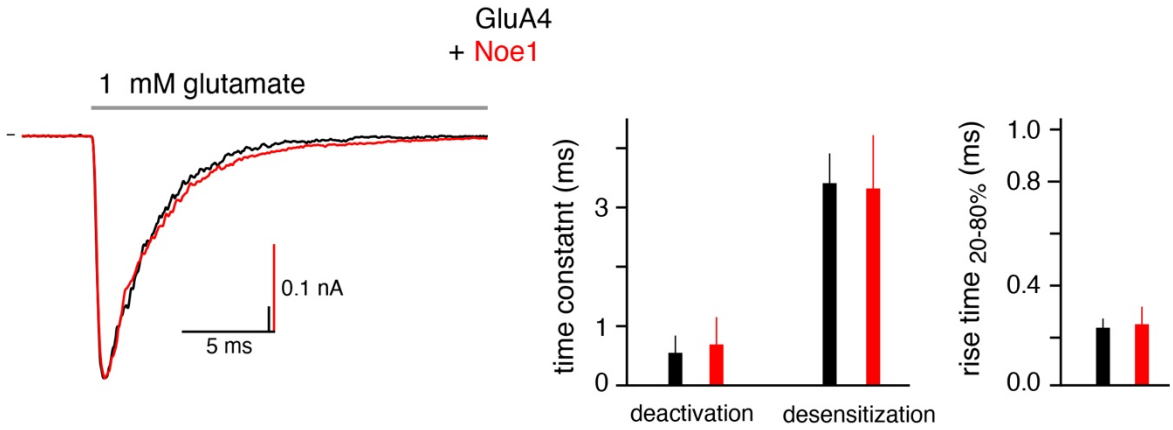


**Figure S14**

**Gating kinetics of GluA4 AMPARs are unaltered by bound Noe1.**

(related to STAR Methods, Discussion)

Left panel, representative current responses to fast 1 mM glutamate-applications recorded in outside-out patches of CHO cells expressing GluA4 AMPARs either alone or together with Noe1. Right panel, bar graph summarizing the parameters of channel gating determined in experiments as on the left. Data are mean ± SD of four patches.